DOI: 10.22226/2410-3535-2018-4-567-571 PACS: 81.00.00

Superplastic behavior of the fine-grained Ti-21Al-18Nb-1Mo-2V-0.3Si intermetallic alloy

S. J. Qu[1], A. H. Feng[1,†], M. R. Shagiev[2], H. Xie[3], B. B. Li[4], J. Shen[1,5]

[†]aihanfeng@tongji.edu.cn

[1]School of Materials Science and Engineering, Tongji University, Shanghai, 201804, China
[2]Institute for Metals Superplasticity Problems of Russian Academy of Sciences, 39 Khalturin str., Ufa, 450001, Russia
[3]Shenyang National Laboratory for Materials Science, Institute of Metal Research of Chinese Academy of Sciences, Shenyang, 110016, China
[4]Luoyang Sunrui Titanium Precision Casting, Luoyang, 471000, China
[5]College of Mechatronics and Control Engineering, Shenzhen University, Shenzhen, 518060, China

Superplastic behavior of the novel Ti-21Al-18Nb-1Mo-2V-0.3Si intermetallic alloy with rather low density $\rho \approx 5.067$ g/cm^3 was studied. The homogeneous fine-grained microstructure in the alloy, which contained three ordered phases: O (Ti_2AlNb), B2 (Ti-Al-Nb) and α_2 (Ti_3Al), was produced by thermomechanical processing. It included the hot isostatic pressing at 1080°C ($P = 140$ MPa for 6 h), two-step quasi-isothermal forging at 870 – 1060°C, and pack rolling at 930 – 950°C. The fine-grained alloy exhibited high superplastic elongations $\delta > 230\%$ in the temperature range of 875 – 1000°C and at an initial strain rate of 4×10^{-4} s^{-1}. The maximum elongation $\delta = 958\%$ was obtained at 960°C. Microstructure analysis revealed that maximum superplastic elongation was obtained when material had approximately equal content of the main B2- and α_2-phases suggesting that the B2/α_2 phase boundary sliding plays an important role during superplastic deformation. Deviation the Burgers orientation relationships: $(110)_{B2}//(0001)_{\alpha 2}$, $[1\text{-}1\text{-}1]_{B2}//[1\text{-}210]_{\alpha 2}$ pointed out to extensive grain rotation during superplastic flow. The deformation induced grain growth testified to grain boundary migration. Besides, the signs of the O→B2→α_2 phase transformations were also observed after testing at 960°C. The minor content of the O-phase in the Ti_2AlNb-based intermetallic alloy was present at 960°C in the (α_2 + O)-lamellar structure. Crystallographic orientations between the α_2- and the O-phases were found to be $(1010)_{\alpha 2}//(110)_O$, $[0001]_{\alpha 2}//[001]_O$.

Keywords: intermetallics, Ti_2AlNb-based alloy, thermomechanical processing, superplasticity.

1. Introduction

Ti_2AlNb-based intermetallic alloys are considered as attractive materials for aerospace applications due to their desirable properties like a unique combination of strength and ductility, low density, moderate oxidation, good fracture toughness and creep resistance [1 – 3]. Promising Ti_2AlNb-based intermetallics usually contain several ordered phases, such as the orthorhombic O-Ti_2AlNb phase, the body centered cubic B2-phase, and the hexagonal α_2-Ti_3Al phase. These alloys were developed to compete and replace nickel-based superalloys in advanced turbine engines and hypersonic vehicles operating at temperatures of 500 – 700°C. In assessing the challenges associated with Ti_2AlNb-based intermetallics, the following issues are worth noting. First, the density of these intermetallics is rather high ($\rho \approx 5.5$ g/cm^3) due to the high content of niobium. Therefore, optimization of the chemical composition in order to decrease the density and increase the specific strength is of a great importance. This can be achieved by partial substitution of niobium with stronger β-stabilizing elements such as molybdenum and vanadium [3]. The second limiting factor for commercial application of Ti_2AlNb-based alloys is the presence of ordered phases which makes these materials hard-to-deform [5 – 9]. Thus, the workability improvement, and even achieving superplasticity for their secondary processing, is also an important issue. It may be realized through the microstructure refinement [10 – 12].

For the recent two decades many researchers studied superplasticity of Ti_2AlNb-based intermetallics. Rosenberg and Mukherjee reported the superplastic properties of the (O + B2)-phase Ti-22Al-26Nb alloy [13]. Jobart and Blandin observed the weakening of the initial rolling texture of the Ti-25Al-10Nb-3V-1Mo alloy during superplastic deformation [14]. Wu and Koo also studied the effect of texture on superplasticity of the Ti-25Al-10Nb alloy [15]. Kim et. al. obtained on the Ti-24Al-11Nb alloy the maximum elongation of 1280% at 970°C and an initial strain rate of 10^{-3} s^{-1} [16]. They also found that the α_2/α_2 grain boundaries and/or the α_2/B2 phase boundaries play a major role in superplastic deformation [16].

The aim of the present paper was to check whether the novel Ti_2AlNb-based alloy with optimized chemical composition, which provided rather low density, would possess good superplastic properties; and if so, determine the temperature interval of superplasticity and evaluate the behavior of different phases during superplastic deformation.

2. Experimental

The Ti_2AlNb-based alloy with developed chemical composition of Ti-21Al-18Nb-1Mo-2V-0.3Si (at. %) was produced by induction skull melting. Its exact chemical composition is given in Table 1. The density of the alloy was measured to be $\rho = 5.067$ g/cm^3.

Table 1. Chemical composition of the novel Ti_2AlNb-based alloy.

Alloying elements, at. %					
Ti	Al	Nb	Mo	V	Si
Bal.	20.87	18.23	0.90	1.74	0.31

The ingot with sizes of 120 mm in diameter and 185 mm in length was subjected to hot isostatic pressing at 1080°C and $P = 140$ MPa for 6 h with subsequent furnace cooling. Then the ingot was sealed in stainless steel can, preheated in electric furnace at 1060°C, and uniaxially compressed with an initial strain rate of 1×10^{-2} s^{-1} to 60%. The temperature of the forging dies was 900°C. After decanning, the forged billet was cut into 2 pieces, heated to 960°C, and subjected to the second compression along the direction, which was perpendicular to the primary compression axis. The temperature of the forging dies during the second deformation step was 870°C. The performs were strained to 70% with an initial strain rate of 1×10^{-2} s^{-1}. The sheets with sizes of $464 \times 180 \times 1.3$ mm^3 were produced by pack rolling of forged preforms at temperatures of 930 – 950°C. In order to decrease the level of thermal stresses the sheets were annealed at 800°C for 40 min.

Microstructure analysis was carried out using FEI Quanta 200 FEG scanning electron microscope with OIM software and FEI TECHAI G2 F30 high-resolution transmission electron microscope. Electropolishing of thin foils and specimens for electron backscattered diffraction (EBSD) analysis was performed in a solution of 6% perchloric acid, 34% n-butyl alcohol, and 60% methanol electrolyte at 45V and –30°C.

Tensile properties of flat specimens with a gauge size of $15 \times 4 \times 1$ mm^3 cut from the hot rolled sheet were studied in the temperature range of 850 – 1000°C and an initial strain rate of 4×10^{-4} s^{-1} using the Instron 5500R testing machine. The tensile axis of the specimens was parallel to the rolling direction of the sheets. In order to minimize oxidation, the gauge sections of specimens were coated with the K-01 glass slurry. Prior to tensile testing, specimens were kept at testing temperature for 5 minutes.

3. Results and discussion

Fig. 1 shows the microstructure of cast and hot isostatically pressed alloy. Optical microscopy revealed equiaxed coarse grains with sizes 500 – 2000 μm (Fig. 1a). SEM analysis has found that those grains consisted mainly of a mixture of the O- and the B2-phases (grey and light color in Fig. 1b, respectively) with the plate-like precipitates of the α_2-phase particles (dark color in Fig. 1b).

Fig. 2a shows the refined microstructure of the alloy in as-rolled condition. One can see the micron-sized grains of the matrix O-phase formed due to occurrence of dynamic recrystallization and the equiaxed particles of the B2- and the α_2-phases with crystallographic orientations between them $(110)_{B2}//(0001)_{\alpha 2}$, $[1\text{-}1\text{-}1]_{B2}//[1\text{-}210]_{\alpha 2}$ (Fig. 2b).

Photograph image of the sheet specimens tested at different temperatures is given in Fig. 3a. The fine-grained intermetallic alloy exhibited high superplastic elongations $\delta > 230\%$ in the temperature range of 875 – 1000°C. During testing with an initial strain rate of 4×10^{-4} s^{-1}, the alloy possessed the highest elongation $\delta = 958\%$ at 960°C. The engineering stress-strain curves of the alloy are shown in Fig. 3b. The flow stress decreased with increasing the testing temperature. Duration of the steady-state flow stage first extended with increasing the testing temperature up to 960°C, and then began to decrease (Fig. 3b). At 960°C, the strain rate sensitivity coefficient for Ti_2AlNb-based alloy exceeded 0.33 at strain rates of $2 \times 10^{-4} – 2 \times 10^{-3}$ s^{-1}.

Fig. 4 presents the EBSD analysis data from three characteristic areas of the specimen tensile tested at 960°C ($\delta = 958\%$). Position "a" was in the grip section of the specimen and this area was subjected only to static annealing, without deformation. Position "b" corresponded to the middle of the gauge section of the specimen; this area was subjected to intermediate straining. Position "c" was near the fracture tip of the specimen, where the maximum strain was observed.

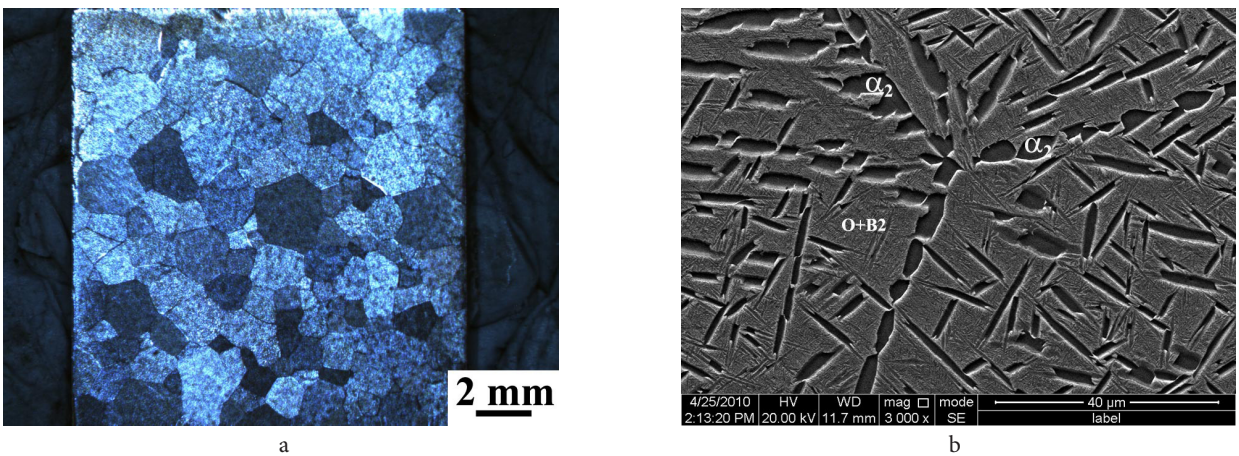

a b

Fig. 1. Microstructure of the cast and hot isostatically pressed alloy: stereoscopic optical image (a), SEM backscattered electron micrograph (b).

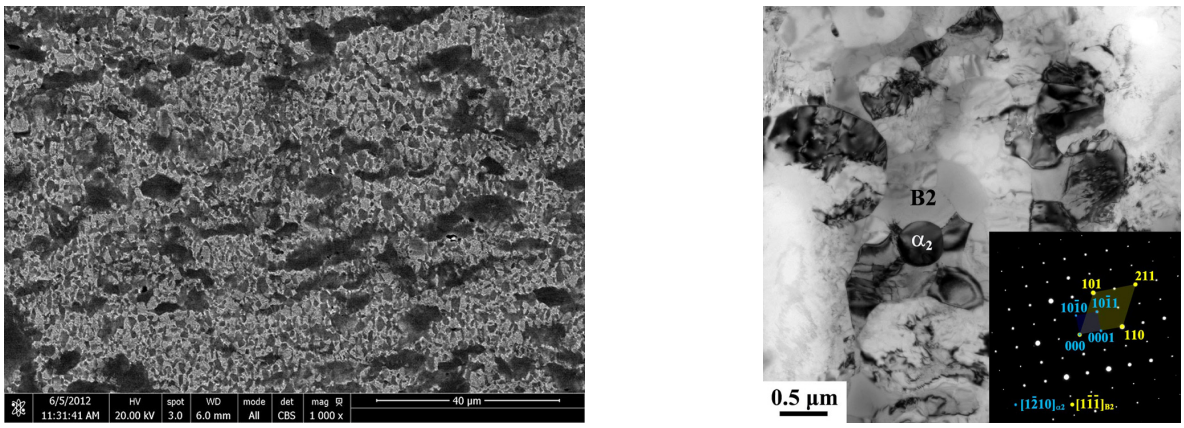

a b

Fig. 2. Microstructure of the sheet: SEM backscattered electron micrograph (a), bright field TEM image and corresponding selected area electron diffraction pattern (b).

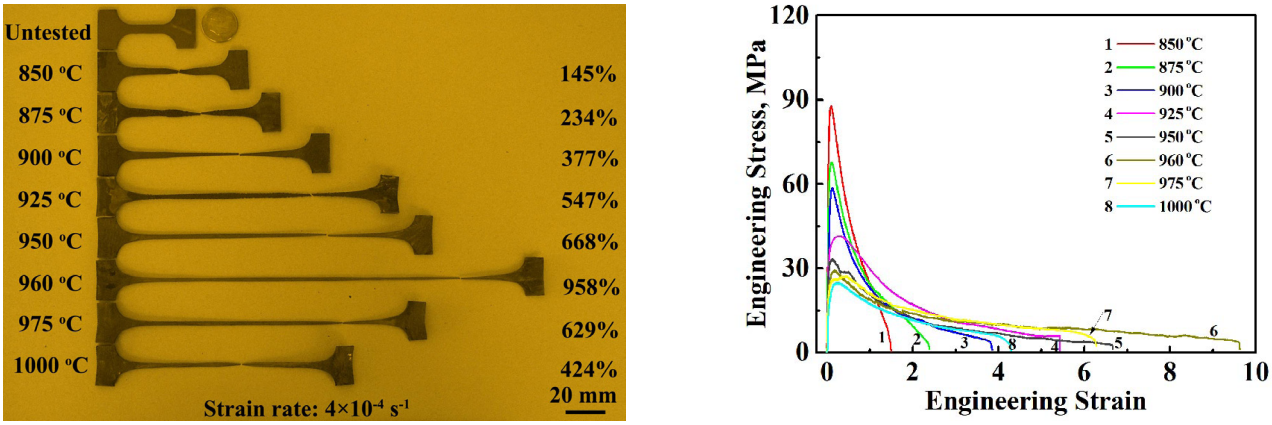

a b

Fig. 3. Photograph image of tensile specimens after testing at 850 – 1000°C with an initial strain rate of 4×10^{-4} s^{-1} (a), engineering stress-strain curves of the alloy (b).

EBSD maps showing the morphology and distribution of different phases in characteristic areas are given in Fig. 4b – d. After testing at 960°C, microstructure of the Ti_2AlNb-based alloy became essentially two-phase (B2 + α_2) with a very small amount of the O-phase. According to phase diagram [2], this corresponds to the high-temperature phase composition of the alloy and testifies to the fast cooling of the specimen from the testing temperature. The ratio of the B2- and α_2-phases varied within the deformed specimen and in the middle of the gauge section it was close to 50:50 (~57:43, whereas in the grip section of the specimen it was ~67:33). Similar results were also reported in [10,16 – 18]. Because of approximately equal ratio of constituent phases, it may be assumed that sliding along the B2/α_2 phase boundaries plays an important role during superplastic deformation of the Ti_2AlNb-based alloy.

Fig. 4e – g shows the distribution of grain sizes within the α_2- and the B2-phases in different characteristic areas. In the grip section of the specimen which was subjected to static annealing only, the average size of the α_2 grains was ~1.6 µm and the average size of the B2 grains was ~2.4 µm (Fig. 4e). In the gauge section of the specimen the deformation induced grain growth was observed, and the average size of α_2 grains was measured to be ~2.0 – 2.1 µm while the average size of the B2 grains was within 3.3 – 3.4 µm (Fig. 4f – g).

Fig. 4h shows the distributions of misorientation angles of the B2- and the α_2-phases in different characteristic areas. A prominent peak at 45° was observed indicating that crystallographic orientations between the B2- and the α_2-phases follow the Burgers orientation relationships: $(110)_{B2}//(0001)_{\alpha 2}$, $[1\text{-}1\text{-}1]_{B2}//[1\text{-}210]_{\alpha 2}$. Peak of misorientation angles near the fracture tip of specimen was slightly shifted to lower angles (~43°) suggesting that extensive grain rotation during superplastic deformation would reduce the Burgers orientation relationships.

TEM images taken from position "b" of the specimen tested in the optimum superplastic conditions are shown in Fig. 5. One can see the equiaxed grains of the B2- and the α_2-phases (Fig. 5a). The high dislocation density was observed within the α_2-grains and in the grain boundary regions. TEM analysis also revealed the small amount of the O-phase which, together with the α_2-phase, formed the (α_2 + O) lamellar structure (Fig. 5b). Crystallographic orientations between the α_2- and O-phases were found to be $(1010)_{\alpha 2}//(110)_O$, $[0001]_{\alpha 2}//[001]_O$ (Fig. 5c – d).

The important role of grain/phase boundary sliding in superplasticity is widely recognized [10,17 – 19]. Grain/phase boundary sliding, grain rotation, and grain boundary migration are the main processes during superplasticity [10,17,19]. The results of the present work also support this

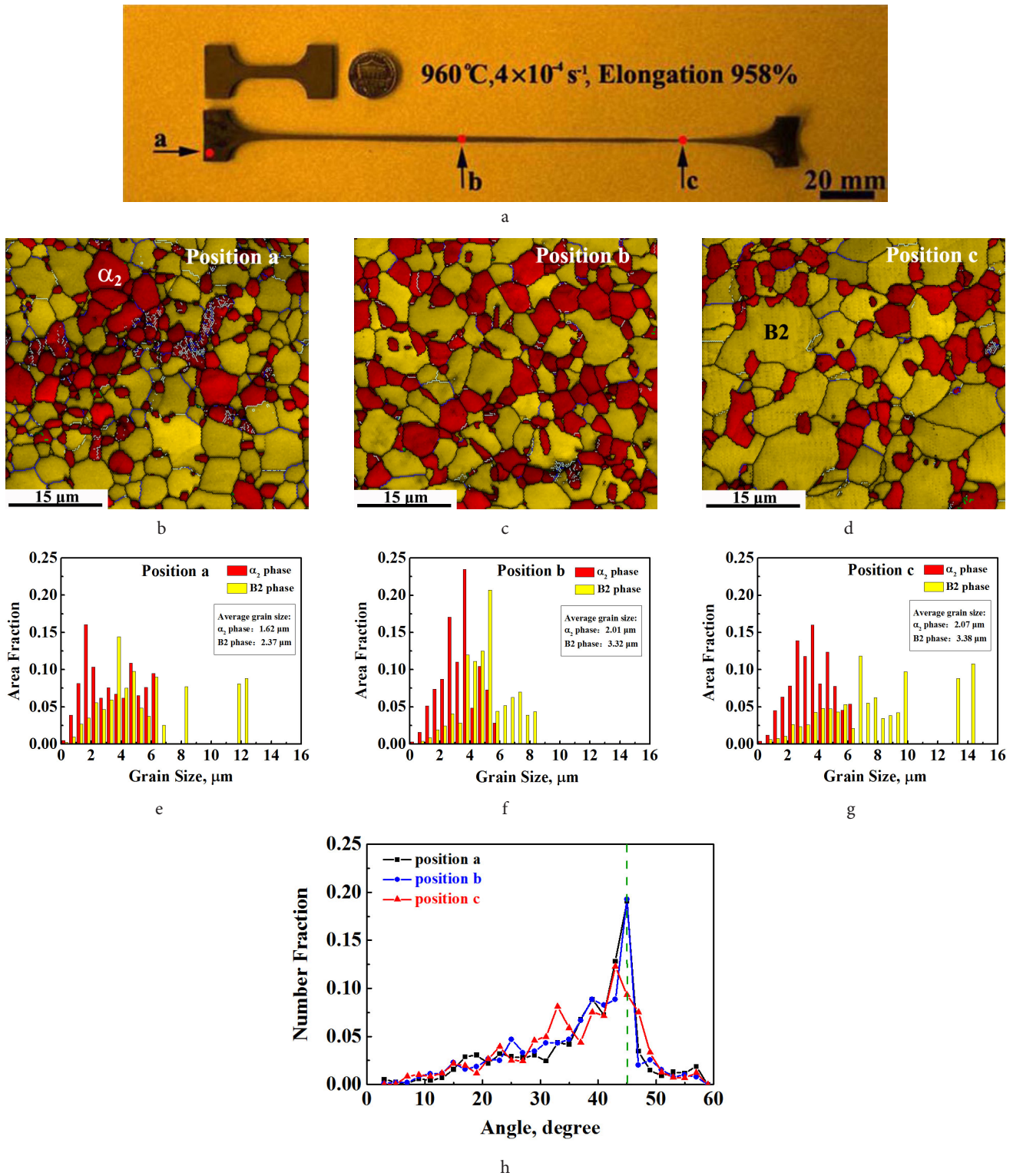

Fig. 4. EBSD analysis data of the specimen tested in the optimum superplastic conditions: photograph image of the tested specimen showing three characteristic areas for microstructure analysis (a); EBSD maps (b – d), distributions of grain sizes (e – g), and distributions of misorientation angles of the B2- and the α_2-phases plotted for different characteristic areas of the specimen (h).

observation for the Ti_2AlNb-based alloy. Close content of the B2- and the α_2-phases (Fig. 4c) suggests that the phase boundary sliding plays an important role during superplastic deformation of this alloy at 960°C. Deviation of the peak of misorientation angles of the B2- and the α_2-phases from 45° (Fig. 4h) points out to extensive grain rotation. The deformation induced grain growth (Fig. 4e – g) testifies to grain boundary migration. Besides, the higher volume fraction of the α_2-phase in the gauge section of the specimen as compared to that in the grip section (Fig. 4b – c) and small amount of the O-phase (Fig. 4b – d and 5b) indicated to occurrence of the O→B2→α_2 phase transformations at testing temperatures that may be beneficial for superplasticity and increase the superplastic elongations [17,20].

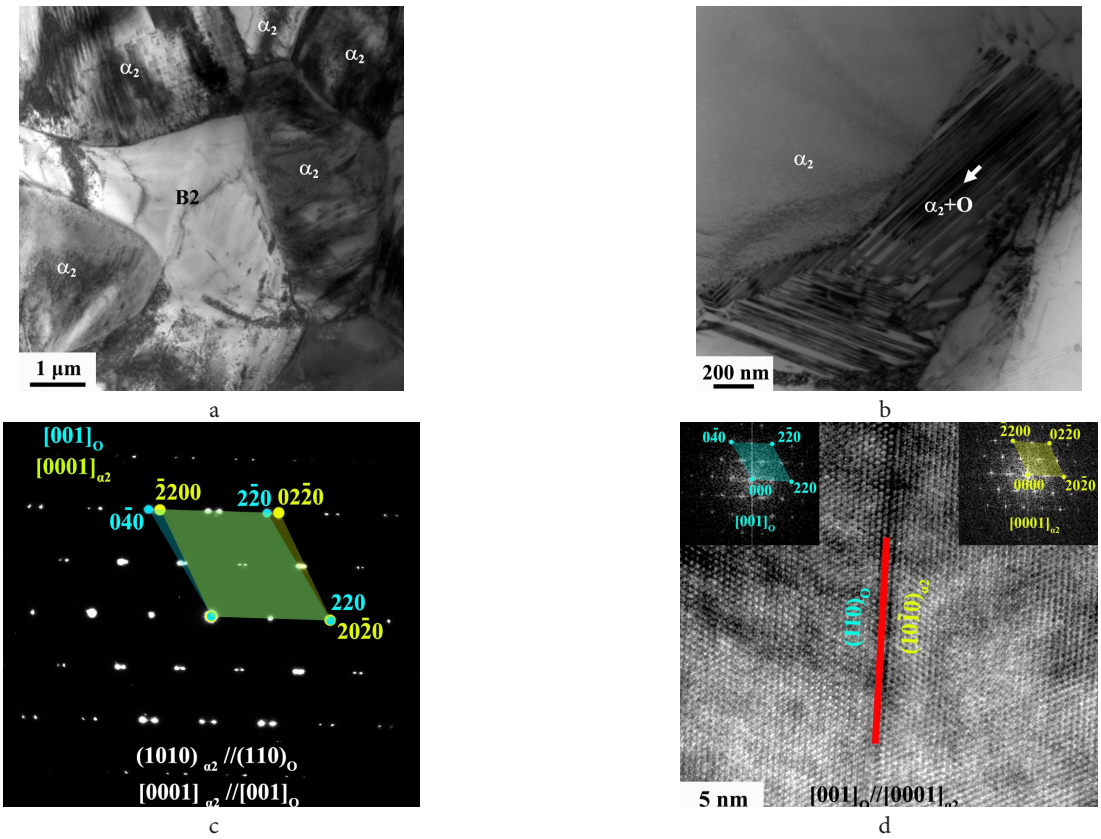

Fig. 5. Microstructure in the middle of the gauge section of the specimen tested at 960°C: bright field TEM images showing the different phases (a – b); selected area electron diffraction pattern corresponding to the lamellar area indicated by arrow in (b) (c); high-resolution TEM image of the area indicated by arrow in (b), the interface was observed along the $[001]_O // [0001]_{\alpha 2}$ zone axis (d).

4. Conclusions

The fine-grained Ti-21Al-18Nb-1Mo-2V-0.3Si intermetallic alloy exhibited superplastic behavior in the temperature range of 875 – 1000°C. At a strain rate of 4×10^{-4} s^{-1}, the alloy possessed the highest elongation $\delta = 958\%$ at 960°C.

Microstructure analysis revealed that under the optimum superplastic conditions the B2/α_2 phase boundary sliding played an important role during superplastic deformation of the Ti_2AlNb-based alloy. At 960°C, the deformation induced grain growth along with the signs of extensive grain rotation and the O→B2→α_2 phase transformations were also observed.

Acknowledgments. The authors are grateful for the financial support provided by the National Natural Science Foundation of China (NSFC) through grants 51871168 and U1302275. The work of M. R. Shagiev was carried out within the state assignment of IMSP RAS.

References

1. D. Banerjee, A. K. Gogia, T. K. Nandi, V. A. Joshi. Acta Metall. 36, 871 (1988).
2. D. Banerjee. Prog. Mater. Sci. 42, 135 (1997).
3. J. M. Xiang, G. B. Mi, S. J. Qu, X. Huang, Z. Chen, A. H. Feng, J. Shen, D. L. Chen. Scientific Reports. 8, 12761 (2018).
4. F. Tang, S. Nakazawa, M. Hagiwara. Mater. Sci. Eng. A. 329 – 331, 492 (2002).
5. L. A. Bendersky. Scripta Metall. Mater. 29, 1645 (1993).
6. L. A. Bendersky, A. Roytburd, W. J. Boettinger. Acta Metall. Mater. 42, 2323 (1994).
7. L. A. Bendersky, W. J. Boettinger. Acta Metall. Mater. 42, 2337 (1994).
8. X. Ren, M. Hagiwara. Acta Mater. 49, 3971 (2001).
9. C. J. Boehlert. Mater. Sci. Eng. A. 279, 118 (2000).
10. O. A. Kaibyshev. Superplasticity of Alloys, Intermetallides and Ceramics. Berlin, Springer-Verlag (1992) 317 p.
11. M. R. Shagiev, G. A. Salishchev. Mat. Sci. Forum. 584 – 586, 153 (2008).
12. Z. X. Zhang, S. J. Qu, A. H. Feng, J. Shen. Mater. Sci. Eng. A. 692, 127 (2017).
13. Y. Rosenberg, A. K. Mukherjee. Mater. Sci. Eng. A. 192 – 193, 788 (1995).
14. D. Jobart, J. J. Blandin. Mater. Sci. Eng. A. 207, 170 (1996).
15. Y. T. Wu, C. H. Koo. Intermetallics. 5, 29 (1997).
16. J. H. Kim, C. G. Park, T. K. Ha, Y. W. Chang. Mater. Sci. Eng. A. 269, 197 (1999).
17. O. A. Kaibyshev. Plasticity and Superplasticity of Metals. Moscow, Metallurgy (1975) 280 p.
18. W. B. Lee, H. S. Yang, Y. W. Kim, A. K. Mukherjee. Scripta Metall. Mater. 29, 1403 (1993).
19. M. G. Zelin, A. K. Mukherjee. Acta Metall. Mater. 43, 2359 (1995).
20. J. Koike, Y. Shimoyama, I. Ohnuma, T. Okamura, R. Kainuma, K. Ishida, K. Maruyama. Acta Mater. 48, 2059 (2000).